Catal Lett (2009) 128:243–247
DOI 10.1007/s10562-008-9745-5

Effect of Preparation Method of $Co_9Fe_3Bi_1Mo_{12}O_{51}$ on the Catalytic Performance in the Oxidative Dehydrogenation of *n*-Butene to 1,3-Butadiene—Comparison Between Co-Precipitation Method and Citric Acid-Derived Sol–Gel Method

Ji Chul Jung · Howon Lee · In Kyu Song

Received: 15 October 2008 / Accepted: 17 October 2008 / Published online: 11 November 2008

Abstract $Co_9Fe_3Bi_1Mo_{12}O_{51}$ catalysts were prepared by two different methods, and were applied to the oxidative dehydrogenation of *n*-butene to 1,3-butadiene in a continuous flow fixed-bed reactor. $Co_9Fe_3Bi_1Mo_{12}O_{51}$–SG catalyst prepared by a citric acid-derived sol–gel method exhibited a higher yield for 1,3-butadiene than $Co_9Fe_3Bi_1Mo_{12}O_{51}$–CP catalyst prepared by a co-precipitation method. It was revealed that the $Co_9Fe_3Bi_1Mo_{12}O_{51}$–SG catalyst retained abundant oxygen species for the reaction and sufficient adsorption sites for *n*-butene compared to the $Co_9Fe_3Bi_1Mo_{12}O_{51}$–CP catalyst, leading to an enhanced catalytic performance of $Co_9Fe_3Bi_1Mo_{12}O_{51}$–SG in the oxidative dehydrogenation of *n*-butene.

Keywords Multicomponent bismuth molybdate · Citric acid-derived sol–gel method · Co-precipitation method · Oxidative dehydrogenation · 1,3-butadiene

1 Introduction

Multicomponent bismuth molybdates have been widely investigated as efficient catalysts for the oxidative dehydrogenation of *n*-butene to 1,3-butadiene [1–3], and co-precipitation method has been generally employed for the preparation of multicomponent bismuth molybdate catalysts [4]. One of the major problems of co-precipitation method, however, is that all metallic cations are not precipitated at the same pH and temperature [5], implying that multicomponent bismuth molybdate catalysts prepared by a co-precipitation method are not molecularly homogeneous. This leads to low efficiency of metal components in the catalyst and lessens reproducibility of catalyst preparation.

Single-step citric acid-derived sol–gel method has attracted much attention as a promising method for preparing fine metal oxide catalysts with high purity, high homogeneity, and high surface area [6–11]. By this method, metal precursors can be blended at molecular level through the formation of metal-citrate complexes [12]. Therefore, it is expected that a multicomponent bismuth molybdate catalyst prepared by a citric acid-derived sol–gel method would show an excellent catalytic performance in the oxidative dehydrogenation of *n*-butene.

Multicomponent bismuth molybdate catalysts have a general form of $M^{II}_aM^{III}_bBi_cMo_dO_e$, which includes divalent metal (M^{II}), trivalent metal (M^{III}), bismuth, and molybdenum [13, 14]. Although a number of multicomponent bismuth molybdate catalysts can be formed depending on the constituent metal components and their compositions [15–18], it has been reported that $Co_9Fe_3Bi_1Mo_{12}O_{51}$ served as an efficient catalyst for the oxidative dehydrogenation of *n*-butene [19, 20]. In this work, therefore, $Co_9Fe_3Bi_1Mo_{12}O_{51}$ was chosen as a model catalyst to see the effect of preparation method on the catalytic performance in the oxidative dehydrogenation of *n*-butene.

For this purpose, $Co_9Fe_3Bi_1Mo_{12}O_{51}$ catalysts were prepared by a co-precipitation method and by a citric acid-derived sol–gel method. They were then applied to the oxidative dehydrogenation of *n*-butene to 1,3-butadiene. The effect of preparation method on the catalytic property and catalytic activity of $Co_9Fe_3Bi_1Mo_{12}O_{51}$ catalysts was investigated.

J. C. Jung · H. Lee · I. K. Song (✉)
School of Chemical and Biological Engineering, Institute of Chemical Processes, Seoul National University, Shinlim-dong, Kwanak-ku, Seoul 151-744, Korea
e-mail: inksong@snu.ac.kr

2 Experimental

2.1 Preparation of $Co_9Fe_3Bi_1Mo_{12}O_{51}$–CP and $Co_9Fe_3Bi_1Mo_{12}O_{51}$–SG Catalysts

$Co_9Fe_3Bi_1Mo_{12}O_{51}$ catalyst was prepared by a co-precipitation method. 1.5 g of bismuth nitrate ($Bi(NO_3)_3 \cdot 5H_2O$, Sigma-Aldrich) was dissolved in 10 mL of distilled water that had been acidified with 3 mL of concentrated nitric acid. The solution was then added into 100 mL of an aqueous solution containing 7.9 g of cobalt nitrate ($Co(NO_3)_2 \cdot 6H_2O$, Sigma-Aldrich) and 3.7 g of ferric nitrate ($Fe(NO_3)_3 \cdot 9H_2O$, Sigma-Aldrich) to obtain a mixed nitrate solution. The mixed nitrate solution was added dropwise into 50 mL of an aqueous solution containing 6.4 g of ammonium molybdate ($(NH_4)_6Mo_7O_{24} \cdot 4H_2O$, Sigma-Aldrich) under vigorous stirring. After stirring the mixed solution vigorously at room temperature for 1 h, a solid product was obtained by evaporation. The solid product was dried overnight at 175 °C, and it was then calcined at 475 °C for 5 h in an air stream to yield a $Co_9Fe_3Bi_1Mo_{12}O_{51}$ catalyst. The catalyst prepared by a co-precipitation method was denoted as $Co_9Fe_3Bi_1Mo_{12}O_{51}$–CP.

$Co_9Fe_3Bi_1Mo_{12}O_{51}$ catalyst was also prepared by a citric acid-derived sol–gel method. 6.4 g of ammonium molybdate ($(NH_4)_6Mo_7O_{24} \cdot 4H_2O$, Sigma-Aldrich) was dissolved in 20 mL of distilled water. 15.9 g of citric acid monohydrate ($C_6H_8O_7 \cdot H_2O$, Sigma-Aldrich) was separately dissolved in 20 mL of distilled water. After mixing these two solutions, 7.9 g of cobalt nitrate ($Co(NO_3)_2 \cdot 6H_2O$, Sigma-Aldrich) and 3.7 g of ferric nitrate ($Fe(NO_3)_3 \cdot 9H_2O$, Sigma-Aldrich) were successively added into the mixed solution to form a transparent solution (Solution A). 1.5 g of bismuth nitrate ($Bi(NO_3)_3 \cdot 5H_2O$, Sigma-Aldrich) was dissolved in 15 mL of distilled water that had been acidified with 10 mL of concentrated nitric acid (Solution B). Solution B was then added dropwise into Solution A under vigorous stirring. After stirring the resulting solution at room temperature for 1 h, it was evaporated to obtain a gel. The gel was then dried overnight at 175 °C to form a xerogel. After glinding the xerogel, it was calcined at 475 °C for 5 h in an air stream to yield a $Co_9Fe_3Bi_1Mo_{12}O_{51}$ catalyst. The catalyst prepared by a citric acid-derived sol–gel method was denoted as $Co_9Fe_3Bi_1Mo_{12}O_{51}$–SG.

2.2 Characterization

Formation of $Co_9Fe_3Bi_1Mo_{12}O_{51}$ catalysts was confirmed by XRD (MAC Science, M18XHF-SRA) measurements. Atomic ratios of constituent metal components in the prepared catalysts were determined by ICP-AES (Shimadz, ICP-1000IV) analyses. Surface areas of the catalysts were measured using a BET apparatus (Micromeritics, ASAP 2010). Surface morphologies of $Co_9Fe_3Bi_1Mo_{12}O_{51}$ catalysts were examined by FE-SEM analyses (Jeol, JSM-6700F). *n*-Butene-TPD (temperature-programmed desorption) experiments were conducted to determine the adsorption ability of $Co_9Fe_3Bi_1Mo_{12}O_{51}$ catalysts for *n*-butene.

2.3 Oxidative Dehydrogenation of *n*-Butene

Oxidative dehydrogenation of *n*-butene to 1,3-butadiene was carried out in a continuous flow fixed-bed reactor in the presence of air and steam. Each catalyst (0.15 g) was charged into a tubular quartz reactor and pretreated at 470 °C for 1 h with an air stream (16 mL/min). Volume of each catalyst bed was maintained at 0.5 mL by introducing quartz sand, in order to conduct the catalytic reaction at the same GHSV (gas hourly space velocity). Water was sufficiently vaporized by passing through a pre-heating zone and was continuously fed into the reactor together with *n*-butene and air. Feed composition was fixed at *n*-butene:O_2:steam = 1:0.75:15. C_4 raffinate-3 containing 57.9 wt.% *n*-butene (1-butene (7.5 wt.%) + *trans*-2-butene (33.9 wt.%) + *cis*-2-butene (16.5 wt.%)) was used as a *n*-butene source, and air was used as an oxygen source (nitrogen in air served as a carrier gas). C_4 raffinate-3 was composed of 57.9 wt.% *n*-butene, 41.6 wt.% *n*-butane, 0.3 wt.% cyclobutane, 0.1 wt.% methyl cyclopropane, and 0.1 wt.% residue. The catalytic reaction was carried out at 420 °C. The contact time was maintained at 14.1 g-catalyst-h/*n*-butene-mole. The catalytic reaction was also conducted in the absence of oxygen feed to measure the oxygen capacity of the catalyst (the amount of oxygen in the catalyst consumed for the oxidative dehydrogenation of *n*-butene to 1,3-butadiene). Reaction products were periodically sampled and analyzed with gas chromatographs. Conversion of *n*-butene and selectivity for 1,3-butadiene were calculated on the basis of carbon balance as follows. Yield for 1,3-butadiene was calculated by multiplying conversion and selectivity.

$$\text{Conversion of } n\text{ - butene} = \frac{\text{moles of } n\text{ - butene reacted}}{\text{moles of } n\text{ - butene supplied}}$$

$$\text{Selectivity for } 1,3\text{ - butadiene} = \frac{\text{moles of } 1,3\text{ - butadiene formed}}{\text{moles of } n\text{ - butene reacted}}$$

3 Results and Discussion

3.1 Formation and Characterization of $Co_9Fe_3Bi_1Mo_{12}O_{51}$ Catalysts

Successful formation of $Co_9Fe_3Bi_1Mo_{12}O_{51}$–CP and $Co_9Fe_3Bi_1Mo_{12}O_{51}$–SG catalysts was confirmed by XRD and ICP-AES measurements. Figure 1 shows the XRD

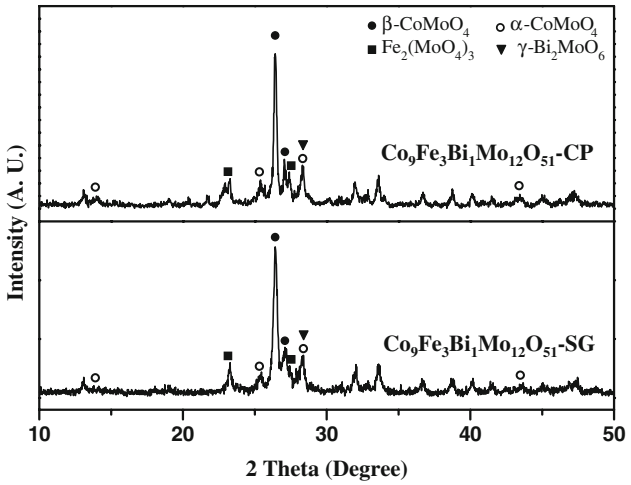

Fig. 1 XRD patterns of $Co_9Fe_3Bi_1Mo_{12}O_{51}$–CP and $Co_9Fe_3Bi_1Mo_{12}O_{51}$–SG catalysts

patterns of $Co_9Fe_3Bi_1Mo_{12}O_{51}$–CP and $Co_9Fe_3Bi_1Mo_{12}O_{51}$–SG catalysts. Each phase was identified by its characteristic diffraction peaks using JCPDS. It was found that both catalysts were composed of four major mixed phases of β-$CoMoO_4$, α-$CoMoO_4$, $Fe_2(MoO_4)_3$, and γ-Bi_2MoO_6, indicating successful formation of $Co_9Fe_3Bi_1Mo_{12}O_{51}$ catalysts [4]. It should be noted that XRD patterns of both catalysts were almost identical. This implies that formation of metal molybdates in the catalyst was independent of the preparation method.

Atomic ratios of constituent metal components determined by ICP-AES analyses are summarized in Table 1.

Table 1 Atomic ratios and BET surface areas of $Co_9Fe_3Bi_1Mo_{12}O_{51}$–CP and $Co_9Fe_3Bi_1Mo_{12}O_{51}$–SG catalysts

Catalyst	Atomic ratio				BET surface area (m^2/g)
	Co	Fe	Bi	Mo	
$Co_9Fe_3Bi_1Mo_{12}O_{51}$–CP	9.0	3.2	1.0	11.4	2.3
$Co_9Fe_3Bi_1Mo_{12}O_{51}$–SG	9.1	2.9	1.0	12.0	9.4

Atomic ratios of Co:Fe:Bi:Mo in both catalysts were almost the same, and these values were well consistent with the theoretical value (Co:Fe:Bi:Mo = 9:3:1:12). This result also supports that $Co_9Fe_3Bi_1Mo_{12}O_{51}$ catalysts were successfully prepared in this work.

BET surface areas of the catalysts are also listed in Table 1. BET surface area of $Co_9Fe_3Bi_1Mo_{12}O_{51}$–SG catalyst (9.4 m^2/g) was much higher than that of $Co_9Fe_3Bi_1Mo_{12}O_{51}$–CP catalyst (2.3 m^2/g). This indicates that the citric acid-derived sol–gel method was more efficient than the co-precipitation method for the preparation of $Co_9Fe_3Bi_1Mo_{12}O_{51}$ catalyst with high surface area [10, 11].

Figure 2 shows the SEM images of $Co_9Fe_3Bi_1Mo_{12}O_{51}$–CP and $Co_9Fe_3Bi_1Mo_{12}O_{51}$–SG catalysts. The images clearly showed a significant difference in surface morphology between two catalysts. It is noteworthy that $Co_9Fe_3Bi_1Mo_{12}O_{51}$–SG catalyst was a plate-like powder, indicating that high surface area of $Co_9Fe_3Bi_1Mo_{12}O_{51}$–SG catalyst was due to the formation of plate-like surface morphology. It can be inferred that $Co_9Fe_3Bi_1Mo_{12}O_{51}$–SG catalyst would provide abundant adsorption sites for *n*-butene in the catalytic reaction due to its high surface area.

3.2 Catalytic Performance in the Oxidative Dehydrogenation of *n*-Butene

Figure 3 shows the typical catalytic performance of $Co_9Fe_3Bi_1Mo_{12}O_{51}$–CP and $Co_9Fe_3Bi_1Mo_{12}O_{51}$–SG in the oxidative dehydrogenation of *n*-butene at 420 °C after a 6 h-reaction. In the catalytic reaction, CO_2 was mainly produced as a by-product. Selectivity for 1,3-butadiene over both catalysts was almost the same, while conversion of *n*-butene over $Co_9Fe_3Bi_1Mo_{12}O_{51}$–SG catalyst was much higher than that over $Co_9Fe_3Bi_1Mo_{12}O_{51}$–CP catalyst. As a consequence, the $Co_9Fe_3Bi_1Mo_{12}O_{51}$–SG catalyst exhibited a higher yield for 1,3-butadiene than the $Co_9Fe_3Bi_1Mo_{12}O_{51}$–CP catalyst. This indicates that the citric acid-derived sol–gel method was more efficient than the co-precipitation method in the preparation of

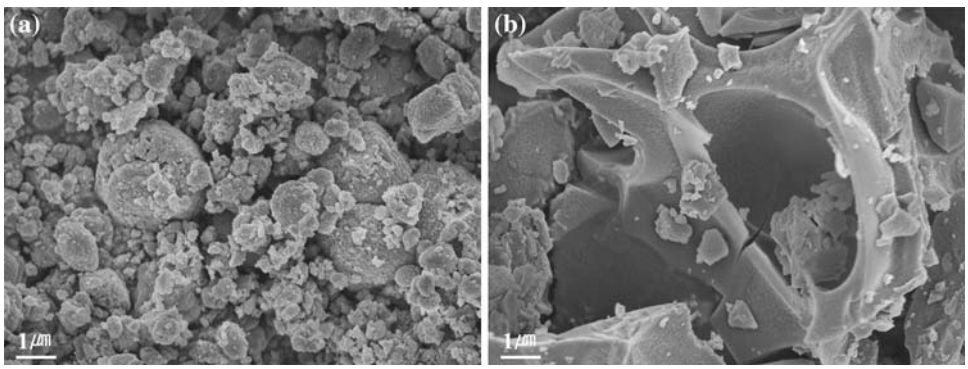

Fig. 2 SEM images of **a** $Co_9Fe_3Bi_1Mo_{12}O_{51}$–CP and **b** $Co_9Fe_3Bi_1Mo_{12}O_{51}$–SG catalysts

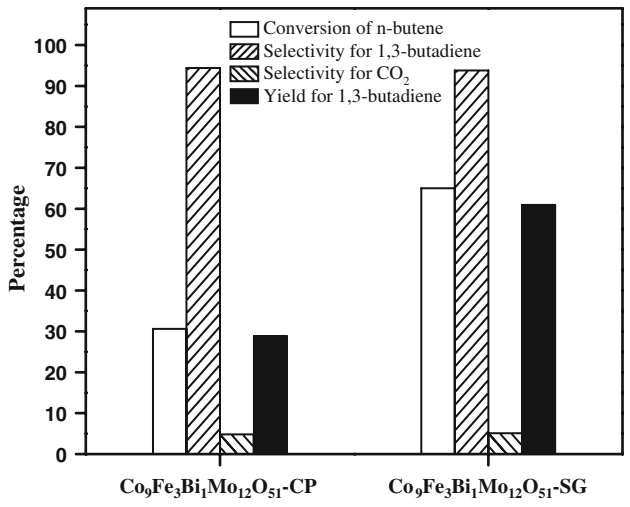

Fig. 3 Catalytic performance of $Co_9Fe_3Bi_1Mo_{12}O_{51}$–CP and $Co_9Fe_3Bi_1Mo_{12}O_{51}$–SG in the oxidative dehydrogenation of *n*-butene to 1,3-butadiene at 420 °C after a 6 h-reaction

$Co_9Fe_3Bi_1Mo_{12}O_{51}$ catalyst for the oxidative dehydrogenation of *n*-butene.

3.3 Oxygen Capacity of $Co_9Fe_3Bi_1Mo_{12}O_{51}$–CP and $Co_9Fe_3Bi_1Mo_{12}O_{51}$–SG Catalysts

Oxidative dehydrogenation of *n*-butene was conducted in the absence of oxygen feed in order to determine the oxygen capacity of the catalyst (the amount of oxygen in the catalyst consumed for the oxidative dehydrogenation of *n*-butene to 1,3-butadiene). Figure 4 shows the yield for 1,3-butadiene over $Co_9Fe_3Bi_1Mo_{12}O_{51}$–CP and $Co_9Fe_3Bi_1Mo_{12}O_{51}$–SG catalysts with time on stream in the absence of oxygen feed in the oxidative dehydrogenation

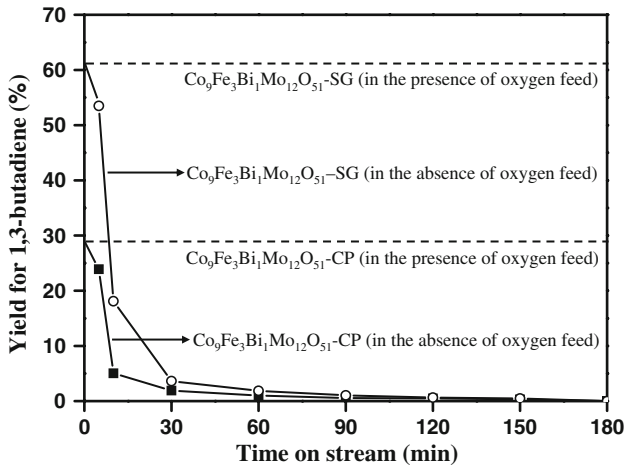

Fig. 4 Yield for 1,3-butadiene over $Co_9Fe_3Bi_1Mo_{12}O_{51}$–CP and $Co_9Fe_3Bi_1Mo_{12}O_{51}$–SG catalysts with time on stream in the absence of oxygen feed in the oxidative dehydrogenation of *n*-butene at 420 °C

of *n*-butene at 420 °C. Yields for 1,3-butadiene in the absence of oxygen feed gradually decreased with increasing reaction time, and finally, reached zero after a 3 h-reaction. This indicates that both catalysts consumed lattice oxygen for the reaction in the absence of oxygen feed, in good agreement with the Mars-van Krevelen mechanism [21–24]. The area obtained by integrating the curve of 1,3-butadiene yield in the absence of oxygen feed reflects the amount of oxygen in the catalyst consumed for the oxidative dehydrogenation of *n*-butene to 1,3-butadiene. Figure 4 clearly shows that the integration area for $Co_9Fe_3Bi_1Mo_{12}O_{51}$–SG catalyst was larger than that for $Co_9Fe_3Bi_1Mo_{12}O_{51}$–CP catalyst. This indicates that the $Co_9Fe_3Bi_1Mo_{12}O_{51}$–SG catalyst retained a larger oxygen capacity than the $Co_9Fe_3Bi_1Mo_{12}O_{51}$–CP catalyst. Therefore, it is believed that the enhanced catalytic performance of $Co_9Fe_3Bi_1Mo_{12}O_{51}$–SG in the oxidative dehydrogenation of *n*-butene was due to the abundant oxygen species for the formation of 1,3-butadiene.

3.4 *n*-Butene-TPD Experiments

Adsorption ability of $Co_9Fe_3Bi_1Mo_{12}O_{51}$–CP and $Co_9Fe_3Bi_1Mo_{12}O_{51}$–SG for *n*-butene was measured by *n*-butene-TPD experiments. Each catalyst (0.15 g) was charged into a conventional TPD apparatus. The catalyst was pretreated at 200 °C for 2 h under a flow of helium (20 mL/min) to remove any physisorbed organic molecules. 20 mL of C_4 raffinate-3 was then pulsed into the reactor every minute at room temperature under a flow of helium (5 mL/min), until the adsorption sites of the catalyst became saturated with *n*-butene. The physisorbed *n*-butene was removed by evacuating the catalyst sample at 50 °C for 1 h. Furnace temperature was increased from room temperature to 500 °C at a heating rate of 5 °C/min under a flow of helium (10 mL/min). The desorbed molecules were detected using a GC-MSD (Agilent, MSD-6890 N GC).

Figure 5 shows the *n*-butene-TPD profiles of $Co_9Fe_3Bi_1Mo_{12}O_{51}$–CP and $Co_9Fe_3Bi_1Mo_{12}O_{51}$–SG catalysts. In the TPD experiments, *n*-butene (1-butene and 2-butene) was not desorbed in its pure form. Instead, the adsorbed *n*-butene was desorbed in the form of 1,3-butadiene and CO_2 by the reaction with oxygen species in the catalyst. In the TPD profiles, the peaks in low temperature region were attributed to the desorbed 1,3-butadiene, while those in high temperature region corresponded to the desorbed CO_2. This result indicates that oxygen species in the catalyst directly reacted with *n*-butene to form 1,3-butadiene and CO_2. It is noticeable that the ratios of 1,3-butadiene peak area with respect to CO_2 peak area over both catalysts were almost identical. This implies that selectivity for 1,3-butadiene and CO_2 over both catalysts would be similar each other. This was well evidenced by the catalytic performance data shown in Fig. 3.

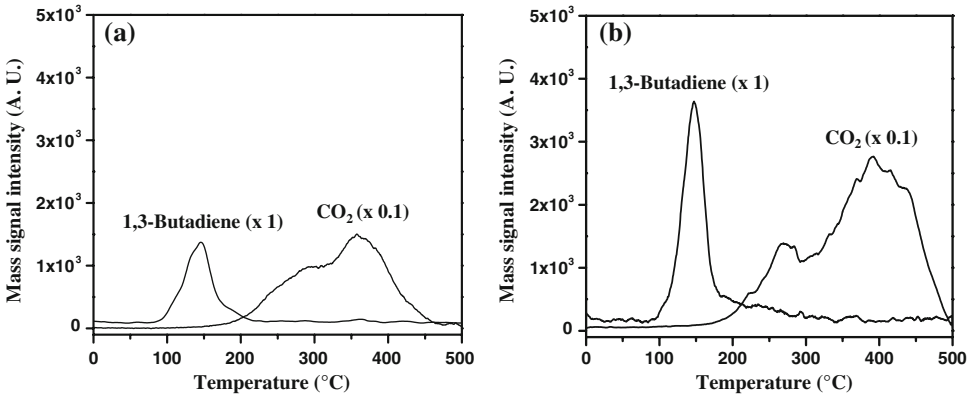

Fig. 5 *n*-Butene-TPD profiles of **a** $Co_9Fe_3Bi_1Mo_{12}O_{51}$–CP and **b** $Co_9Fe_3Bi_1Mo_{12}O_{51}$–SG catalysts

Undoubtedly, the total area of TPD profile reflects the amount of *n*-butene adsorbed on the catalyst. As shown in Fig. 5, the total area of TPD profile for $Co_9Fe_3Bi_1Mo_{12}O_{51}$–SG (Fig. 5b) was much larger than that for $Co_9Fe_3Bi_1Mo_{12}O_{51}$–CP (Fig. 5a), indicating that the $Co_9Fe_3Bi_1Mo_{12}O_{51}$–SG catalyst retained more adsorption sites for *n*-butene on the catalyst surface than the $Co_9Fe_3Bi_1Mo_{12}O_{51}$–CP catalyst. Together with the fact that the $Co_9Fe_3Bi_1Mo_{12}O_{51}$–SG catalyst retained more abundant oxygen species for the oxidative dehydrogenation of *n*-butene to 1,3-butadiene than the $Co_9Fe_3Bi_1Mo_{12}O_{51}$–CP catalyst (Fig. 4), the above result strongly supports the fact that the $Co_9Fe_3Bi_1Mo_{12}O_{51}$–SG catalyst showed a higher conversion of *n*-butene than the $Co_9Fe_3Bi_1Mo_{12}O_{51}$–CP catalyst (Fig. 3). It is concluded that the enhanced catalytic performance of $Co_9Fe_3Bi_1Mo_{12}O_{51}$–SG was attributed to its abundant oxygen species for the reaction and sufficient adsorption sites for *n*-butene on the catalyst surface.

4 Conclusions

$Co_9Fe_3Bi_1Mo_{12}O_{51}$–CP and $Co_9Fe_3Bi_1Mo_{12}O_{51}$–SG catalysts were prepared by a co-precipitation method and by a citric acid-derived sol–gel method, respectively. They were then applied to the oxidative dehydrogenation of *n*-butene to 1,3-butadiene. Yield for 1,3-butadiene over $Co_9Fe_3Bi_1Mo_{12}O_{51}$–SG catalyst was much higher than that over $Co_9Fe_3Bi_1Mo_{12}O_{51}$–CP catalyst, indicating that the citric acid-derived sol–gel method was more efficient than the co-precipitation method in the preparation of $Co_9Fe_3Bi_1Mo_{12}O_{51}$ catalyst for the oxidative dehydrogenation of *n*-butene. Oxidative dehydrogenation of *n*-butene in the absence of oxygen feed and *n*-butene-TPD experiments were conducted over both catalysts, in order to elucidate their different catalytic performance. It was revealed that the $Co_9Fe_3Bi_1Mo_{12}O_{51}$–SG catalyst retained a larger oxygen capacity and much more adsorption sites for *n*-butene than the $Co_9Fe_3Bi_1Mo_{12}O_{51}$–CP catalyst. Therefore, it is concluded that the enhanced catalytic performance of $Co_9Fe_3Bi_1Mo_{12}O_{51}$–SG was attributed to its abundant oxygen species for the reaction and sufficient adsorption sites for *n*-butene on the catalyst surface.

Acknowledgement The authors would like to acknowledge funding from the Korea Ministry of Knowledge Economy (MKE) through "Energy Technology Innovation Program".

References

1. Grasselli RK (2002) Top Catal 21:79–88
2. Batist PhA, Bouwens JFH, Schuit GCA (1972) J Catal 25:1–11
3. Jung JC, Lee H, Kim H, Chung Y-M, Kim TJ, Lee SJ, Oh S-H, Kim YS, Song IK (2008) Catal Lett 124:262–267
4. Moro-oka Y, Ueda W (1994) Adv Catal 40:233–273
5. Kuang W, Fan Y, Chen Y (1999) J Colloid Interface Sci 215:364–369
6. Tanaka Y, Takeguchi T, Kikuchi R, Eguchi K (2005) Appl Catal A 279:59–66
7. Hwang BJ, Santhanam R, Liu DG (2001) J Power Sources 97:443–446
8. Azadmanjiri J (2008) Mater Chem Phys 109:109–112
9. Pajonk GM (1991) Appl Catal 72:217–266
10. Liu S, Xiu Z, Liu J, Xu F, Yu W, Yu J, Feng G (2008) J Alloys Compd 457:L12–L14
11. Liu L, Jiao L, Zhang Y, Sun J, Yang L, Miao Y, Yuan H, Wang Y (2008) Mater Chem Phys 111:565–569
12. Katsuyama S, Takagi Y, Ito M, Majima K, Nagai H, Sakai H, Yoshimura K, Kosuge K (2002) J Appl Phys 92:1391–1398
13. Cullis CF, Hucknall DJ (1982) In: Bond GC, Webb G (eds) A specialist periodical report: catalysis, vol 5. Royal Chem Soc, London, pp 273–307
14. Kung HH, Kung MC (1985) Adv Catal 33:159–198
15. Grasselli RK, Burrington JD (1981) Adv Catal 30:133–163
16. Bettahar MM, Costentin G, Savary L, Lavalley JC (1996) Appl Catal A 145:1–48
17. Han Y-H, Ueda W, Moro-oka Y (1999) J Catal 186:75–80
18. Brazdil JF, Suresh DD, Grasselli RK (1980) J Catal 66:347–367
19. Jung JC, Lee H, Kim H, Chung Y-M, Kim TJ, Lee SJ, Oh S-H, Kim YS, Song IK (2008) Catal Commun 9:1676–1680
20. Jung JC, Lee H, Kim H, Chung Y-M, Kim TJ, Lee SJ, Oh S-H, Kim YS, Song IK (2008) Catal Lett 123:239–245
21. Ruckenstein E, Krishnan R, Rai KN (1976) J Catal 45:270–273
22. Schuit GCA (1974) J Less Comm Metals 36:329–388
23. Ruiz P, Delmon B (1988) Catal Today 3:199–209
24. Ueda W, Moro-oka Y, Ikaws T (1984) J Catal 88:214–221